

# Monitoring the healing of combat wounds using Raman spectroscopic mapping

Nicole J. Crane, PhD<sup>1</sup>; Trevor S. Brown, PhD<sup>1</sup>; Korboi N. Evans, MD<sup>2</sup>; Jason S. Hawksworth, MD<sup>3</sup>; Sean Hussey, MD<sup>4</sup>; Doug K. Tadaki, PhD<sup>1</sup>; Eric A. Elster, MD<sup>1,5,6</sup>

1. Regenerative Medicine Department, Combat Casualty Care, Operational and Undersea Medicine, Naval Medical Research Center, Silver Spring, Maryland,
2. Department of Orthopaedics and Rehabilitation,
3. Department of Surgery, Walter Reed Army Medical Center, Washington, District of Columbia,
4. Department of Pathology, National Naval Medical Center, Bethesda, Maryland,
5. Uniformed Services University of Health Sciences, Bethesda, Maryland, and
6. Department of Surgery, National Naval Medical Center, Bethesda, Maryland

**Reprint requests:**

Eric A. Elster, MD, Regenerative Medicine Department, Combat Casualty Care, Operational and Undersea Medicine, Naval Medical Research Center, Silver Spring, MD 20910.  
Tel: ± 1 301 319 8632;  
Fax: 301 295 1423;  
Email: eric.elster@med.navy.mil

Manuscript received: November 3, 2009  
Accepted in final form: April 1, 2010

DOI:10.1111/j.1524-475X.2010.00597.x

The management of modern traumatic war wounds remains a significant challenge for clinicians. This is a reflection of the extensive osseous and soft-tissue damage caused by blasts and high-energy projectiles.<sup>1</sup> The ensuing inflammatory response ultimately dictates the pace of wound healing and tissue regeneration.<sup>2–3</sup> Consequently, the eventual timing of wound closure or definitive coverage is often subjectively based. In addition, some wounds fail, despite the use and application of novel wound-specific treatment modalities.<sup>3</sup> An understanding of the molecular environment of acute wounds throughout the debridement process can provide valuable insight into the mechanisms associated with the eventual wound outcome.

Wound healing is a complex process dictated by the interactions of inflammatory cells and mediators present within the molecular environment. Acute wounds typically progress through histologic and functionally distinct phases of healing with significant overlap. The initial wound inflammatory response provides the effector molecules and mitogenic factors necessary for cellular migration and the clearance of damaged extracellular matrix (ECM).<sup>4</sup> Angiogenesis and provisional matrix formation then ensues via the activation of macrophages and fibroblasts. The provisional matrix, composed mainly of fibrinogen and hyaluronan, is eventually replaced by a

## ABSTRACT

Soldiers wounded in modern warfare present with extensive and complicated acute wounds, confounded by an overwhelming inflammatory response. The pathophysiology of acute wounds is unknown and timing of wound closure remains subjective. Collagen gene expression profiles are presented for 24 patients. Impaired healing wounds show a twofold decrease in the up-regulation of COL1A1 and COL3A1 genes in the beginning of the wound healing process, compared with normal healing wounds. By the final debridement, however, collagen gene expression profiles for normal and impaired healing wounds are similar for COL1A1 and COL3A1. In addition, Raman spectroscopic maps are collected of biopsy tissue sections, from the first and last debridements of 10 wounds collected from nine patients. Tissue components obtained for the debridement biopsies are compared to elucidate whether or not a wound heals normally. Raman spectroscopy showed a loss of collagen in five patients, indicated by a negative percent difference in the 1,665/1,445 cm<sup>-1</sup> band area ratios. Four healed patients showed an increased or unchanged collagen content. Here, we demonstrate the potential of Raman spectroscopic analysis of wound biopsies for classification of wounds as normal or impaired healing. Raman spectroscopy has the potential to noninvasively monitor collagen deposition in the wound bed, during surgical wound debridements, to help determine the optimal time for wound closure.

stronger and more organized ECM comprised of collagen types III and I and proteoglycans.<sup>5</sup> A sustained proinflammatory state with failure of progression through the latter phases of wound healing is thought to be the underlying mechanism associated with delayed healing and eventual wound failure.<sup>6</sup> Therefore, characterization of the wound composition may lend significant contributions to help distinguish wounds arrested in this inflammatory state.

Raman vibrational spectroscopy offers the capability to accurately detect and identify the various molecules that comprise the ECM during wound healing. It is an imaging technique in which the precise biochemical composition of biologic samples can be obtained via noninvasive and non-destructive means in their native state. It has been proven effective in assessing tissues at the molecular level with diverse clinical and diagnostic applications to include the analysis of cellular structure and the determination of tumor grade and type.<sup>7–23</sup> Pathologic alterations of wounds are accompanied by fundamental changes in the molecular environment that can be analyzed by vibrational spectroscopy.<sup>12,24</sup> The identified changes may provide the objective markers of acute wound healing, which can then be integrated with clinical characteristics to guide the management of traumatic wounds. For instance, changes in collagen vibrational bands could be correlated with

W R R	5 9 7	B	Dispatch: 13.5.10	Journal: WRR	CE:
Journal Name	Manuscript No.		Author Received:	No. of pages: 8	PE: xx



Report Documentation Page			Form Approved OMB No. 0704-0188	
<p>Public reporting burden for the collection of information is estimated to average 1 hour per response, including the time for reviewing instructions, searching existing data sources, gathering and maintaining the data needed, and completing and reviewing the collection of information. Send comments regarding this burden estimate or any other aspect of this collection of information, including suggestions for reducing this burden, to Washington Headquarters Services, Directorate for Information Operations and Reports, 1215 Jefferson Davis Highway, Suite 1204, Arlington VA 22202-4302. Respondents should be aware that notwithstanding any other provision of law, no person shall be subject to a penalty for failing to comply with a collection of information if it does not display a currently valid OMB control number.</p>				
1. REPORT DATE <b>2010</b>	2. REPORT TYPE	3. DATES COVERED <b>00-00-2010 to 00-00-2010</b>		
<b>4. TITLE AND SUBTITLE</b> <b>Monitoring the healing of combat wounds using Raman spectroscopic mapping</b>			5a. CONTRACT NUMBER	
			5b. GRANT NUMBER	
			5c. PROGRAM ELEMENT NUMBER	
<b>6. AUTHOR(S)</b>			5d. PROJECT NUMBER	
			5e. TASK NUMBER	
			5f. WORK UNIT NUMBER	
<b>7. PERFORMING ORGANIZATION NAME(S) AND ADDRESS(ES)</b> <b>Regenerative Medicine Department,,Combat Casualty Care, Operational and Undersea Medicine, Naval Medical Research Center,Silver Spring,MD</b>			8. PERFORMING ORGANIZATION REPORT NUMBER	
<b>9. SPONSORING/MONITORING AGENCY NAME(S) AND ADDRESS(ES)</b>			10. SPONSOR/MONITOR'S ACRONYM(S)	
			11. SPONSOR/MONITOR'S REPORT NUMBER(S)	
<b>12. DISTRIBUTION/AVAILABILITY STATEMENT</b> <b>Approved for public release; distribution unlimited</b>				
<b>13. SUPPLEMENTARY NOTES</b>				
<b>14. ABSTRACT</b> <p><b>Soldiers wounded in modern warfare present with extensive and complicated acute wounds, confounded by an overwhelming inflammatory response. The pathophysiology of acute wounds is unknown and timing of wound closure remains subjective. Collagen gene expression profiles are presented for 24 patients. Impaired healing wounds show a twofold decrease in the up-regulation of COL1A1 and COL3A1 genes in the beginning of the wound healing process compared with normal healing wounds. By the final debridement, however, collagen gene expression profiles for normal and impaired healing wounds are similar for COL1A1 and COL3A1. In addition, Raman spectroscopic maps are collected of biopsy tissue sections, from the first and last debridements of 10 wounds collected from nine patients. Tissue components obtained for the debridement biopsies are compared to elucidate whether or not a wound heals normally. Raman spectroscopy showed a loss of collagen in five patients, indicated by a negative percent difference in the 1,665/1,445cm 1 band area ratios. Four healed patients showed an increased or unchanged collagen content. Here, we demonstrate the potential of Raman spectroscopic analysis of wound biopsies for classification of wounds as normal or impaired healing. Raman spectroscopy has the potential to noninvasively monitor collagen deposition in the wound bed, during surgical wound debridements, to help determine the optimal time for wound closure.</b></p>				
<b>15. SUBJECT TERMS</b>				
<b>16. SECURITY CLASSIFICATION OF:</b> a. REPORT      b. ABSTRACT      c. THIS PAGE <b>unclassified</b> <b>unclassified</b> <b>unclassified</b>			<b>17. LIMITATION OF ABSTRACT</b> <b>Same as Report (SAR)</b>	<b>18. NUMBER OF PAGES</b> <b>8</b>
			<b>19a. NAME OF RESPONSIBLE PERSON</b>	



1  
2  
3  
4  
5  
6  
7  
8  
9  
10  
11  
12  
13  
14  
15  
16  
17  
18  
19  
20  
21  
22  
23  
24  
25  
26  
27  
28  
29  
30  
31  
32  
33  
34  
35  
36  
37  
38  
39  
40  
41  
42  
43  
44  
45  
46  
47  
48  
49  
50  
51  
52  
53  
54  
55  
56  
57  
58  
59  
60  
61  
62  
63  
alterations in collagen deposition and reepithelialization of the wound bed.

The complete pathophysiology of acute wounds and the biochemical mechanisms associated with wound failure remains poorly defined. In the current study, we evaluate gene expression profiles of the wounds, specifically collagens, and demonstrate the feasibility of Raman spectroscopy to acquire detailed structural information from various molecules involved in the process of wound healing. Specifically, the spectral images of wounds that healed uneventfully are compared with wounds that show impaired healing.

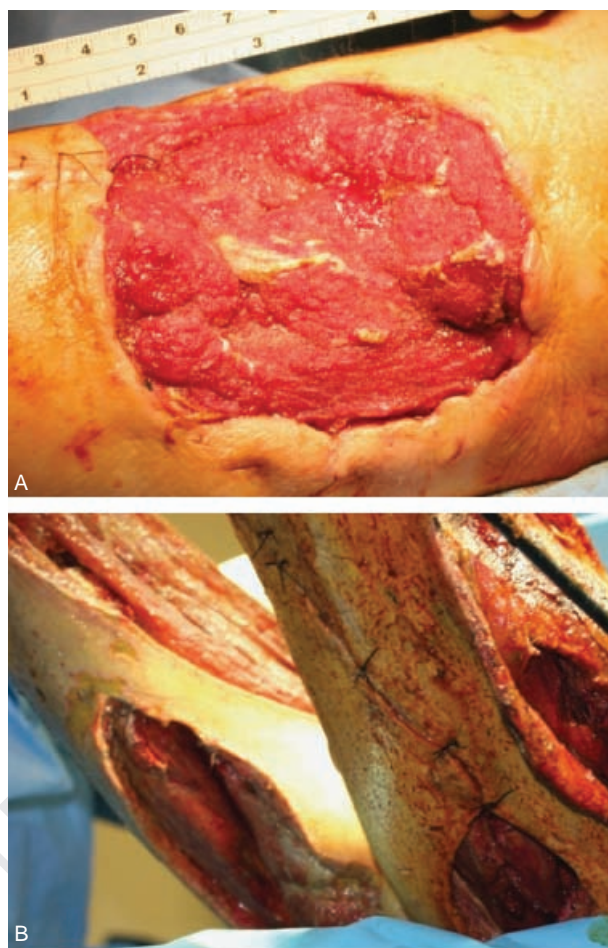
## MATERIALS AND METHODS

### Clinical study

This study was approved by the institutional review board of the National Naval Medical Center (NNMC). All study participants were recruited from wounded Operation Iraqi Freedom and Operation Enduring Freedom U.S. service members evacuated to the National Capital Area. Informed consent was obtained from all participating patients. Inclusion criteria for this study were defined as all service men and women who sustained penetrating injuries to one or more extremities. Exclusions from this study included patients with confounding comorbid conditions such as immune disorders, connective tissue disorders, diabetes mellitus, or any conditions requiring immunosuppressive agents. Table 1 summarizes several demographics for patients with normal and impaired healing wounds.

### Wound treatment

Surgical debridement and pulse lavage were performed in the operating room every 48–72 hours until definitive wound closure or coverage. Wound negative wound pressure therapy was applied to the wounds between surgical debridements, as the per current standard practice at NNMC.<sup>3</sup> All wounds were examined once daily following wound closure or coverage until the sutures were removed. All patients were followed clinically for 30 days. The primary clinical outcome was successful wound healing after definitive closure or coverage (Figure 1A). Impaired wound healing included a delayed wound closure or subsequent wound dehiscence. Delayed wound closure was defined as definitive closure occurring two standard deviations outside of the normal wound closure time period, or ≥21 days after injury. Dehiscence was defined as the spon-



Colour

**Figure 1.** Photographs are shown for a patient with a normal healing wound (A) and impaired healing wounds (B).

taneous partial or complete disruption of a previously closed wound after primary closure or > 90% graft loss after skin grafting (Figure 1B). Wounds that progressed to healing at 30 days and did not necessitate a return to the operating room were considered healed. Timing of closure was at the discretion of the attending surgeon.

### Sample collection

A 1 cm<sup>3</sup> wound tissue specimen was obtained from the center of the wound bed at each debridement and stored in RNA later (Ambion, Austin, TX). All samples were stored at –80°F until analysis.

### Gene expression analysis

The process for tissue gene expression analysis has been discussed in detail.<sup>3</sup> Briefly, the tissue samples were homogenized and total RNA was isolated using Qiagen RNeasy Fibrous Tissue Mini Kit (Qiagen Inc., Valencia, CA) according to the manufacturer's instructions. After assessing RNA purity, quantity, and quality, reverse transcriptions were performed using Roche 1st Strand

**Table 1.**

	Normal healing (n=19)	Impaired healing (n=5)	p-value
Age	23.5 ± 5.5	21.6 ± 2.5	0.508
ISS	18.4 ± 9.1	38.0 ± 10.2	8.80E-05
Days to closure	4.2 ± 2.7	14.1 ± 12.1	0.007
Surface area of wound (cm <sup>2</sup> )	149 ± 94	506 ± 532	0.003

Synthesis kits (Roche Diagnostics Corporation, Indianapolis, IN). Quantitative real-time polymerase chain reaction (QRT-PCR) was performed using the ABI Prism 7900HT Sequence Detection System (Applied Biosystems, Foster City, CA) and custom-designed TaqMan low-density arrays to assess gene transcript expression; all QRT-PCR measurements were performed in duplicate. As an internal control, primers for 18S rRNA were used for each reaction. Fold change in gene expression was calculated using the  $2^{-\Delta\Delta C_T}$  method<sup>25</sup>; values are relative to a pooled control data set.

### Raman spectroscopic mapping

Before Raman spectroscopic mapping, each frozen tissue was transferred to a 1.5 mL cryovial containing 10% neutral buffered formalin for thawing. The tissue was embedded in paraffin, sectioned at 10 µm, and mounted unstained on aluminized glass slides (Fisher Thermo Scientific, Madison, WI). Serial sections, 5 µm thick, were cut and mounted on standard glass slides and stained with hematoxylin & eosin (H&E) for histological evaluation by an experienced pathologist. Unstained sections were deparaffinized with a stirred 40 °C hexane bath for 48 hours and allowed to air dry before spectroscopic examination.

Slides were secured in the microscope slide holder accessory of the Raman Station 400 (Perkin Elmer, Shelton, CT) for Raman map acquisition. Raman map sizes ranged between approximately 8 and 31 mm<sup>2</sup> and contained 238–832 individual Raman spectra. Raman spectra were generated with 100 mW of 785 nm point laser radiation (100 µm spot) every 200 µm over the spectral range of 1,800–500 cm<sup>-1</sup> (4 cm<sup>-1</sup> spectral resolution). Three accumulations of 15-second acquisitions were coadded at each point in the Raman map. Total acquisition times ranged between 3.5 and 13 hours.

### Data analysis

All Raman maps were imported into MATLAB (Mathworks, Natick, MA), where they were subjected to multivariate analysis. Singular value decomposition was applied to all data sets. A Scree plot was used to determine the necessary number of loadings such that 99% of the variance in the data set was described by the chosen loadings. Loadings used for factor analysis were extracted with band target entropy minimization (BTEM)<sup>26–28</sup> and then manually rotated until all factors were nonnegative and their associated score images were nonnegative. Nonnegative factors closely resemble real Raman spectra and can be compared with reference Raman spectra. Nonnegative score images ensure orthogonality of factors and a unique basis set.

Resulting factors representative of the major tissue component were then exported as an ASCII file and imported into Grams/AI software for peak fitting. Factors were automatically intensity normalized to the 1,445 cm<sup>-1</sup> methylene scissoring band and baseline corrected with BTEM, and so additional preprocessing was not necessary for peak fitting. All Raman bands were fit with mixed Gaussian/Lorentzian bands. The fit was considered good when the  $R^2$  value reached at least 0.95.

### Statistical analysis

Fold changes in gene expression profiles between normal and impaired healing wounds were assessed using a Mann–Whitney *U* test. Analyses were performed using SPSS software (SPSS 18.0, SPSS Inc., Chicago, IL). Differences in values were considered statistically significant with a two-tailed *p*-value < 0.05.

## RESULTS

### Pathology of wound tissue biopsy sections

Tissue biopsies taken at the first and last debridements for each wound were stained with H&E. The H&E-stained tissue sections were examined for gross pathology. In general, for normal healing wounds, first debridement biopsies revealed varying degrees of acute chronic inflammation, minimal necrosis, and differing numbers of leukocytes and neutrophils. The final debridement biopsies collected from normal wounds exhibited mild to moderate acute chronic inflammation, fibrosis, and neovascularization. Figure 2A and B show the H&E-stained sections of the first and final debridements of a normal healing wound, respectively. Figure 2A shows severe inflammation, both acute and chronic, minimal necrosis, and muscle atrophy with focal fibrosis. Figure 2B shows fibrosis and mild chronic inflammation, with no residual muscle fibers. Tissue taken at the first debridement contained increased numbers of neutrophils compared with the tissue taken at the final debridement and was generally more inflamed.

Tissue taken at the first debridement of impaired healing wounds showed moderate chronic inflammation, coagulative necrosis, and scattered leukocytes and neutrophils. Tissue taken from the final debridement of impaired healing wounds exhibited fibrosis, and moderate to severe acute chronic inflammation. Figure 2C and D, respectively, also show the H&E-stained sections of the first and final debridements of an impaired healing wound. Figure 2C shows mild acute and chronic inflammation, while Figure 2D shows moderate acute and chronic inflammation, calcification, increased fibroblasts, and focal coagulative necrosis. For the impaired healing wound, the tissue taken at the final debridement shows indications of necrosis and appears more inflamed than the tissue taken at the first debridement. The impaired healing wound shown in Figure 2C and D is an extreme case of impaired healing—the wound dehisced. For other wound biopsies, delineating clear differences in pathology between normal and impaired healing wounds is somewhat challenging.

### Collagen gene expression

Samples from 24 patients were used to examine gross profile changes in gene expression. The mean fold-change in gene expression is shown in Figure 3 for all patients enrolled in the study, with wounds classified as normal healing (black bars) and wounds classified as impaired healing (white bars). Profiles for collagen genes are presented here as collagen is the major tissue component evidenced in the loadings.

Gene expression for type I collagen  $\alpha 1$  (COL1A1) and type III collagen  $\alpha 1$  (COL3A1) in impaired healing wounds is substantially less than that of normal healing

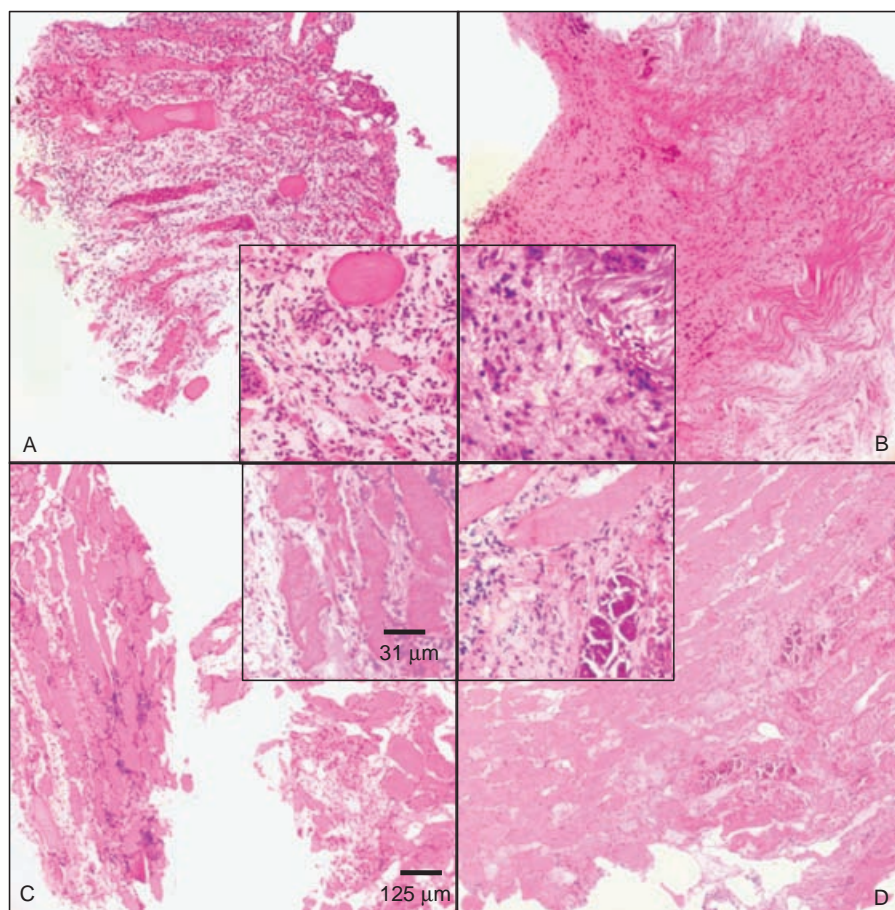


**Figure 2.** Hematoxylin and eosin-stained tissue biopsy sections for a normal healing wound taken at the first (A) and last debridements (B), and an impaired healing wound taken at the first (C) and last (D) debridements. All images are shown at  $\times 10$  magnification with a  $\times 40$  magnification inset.

wounds (Figure 3A). In fact, gene expression of COL1A1 and COL3A1 are twofold reduced in impaired healing wounds compared with normal healing wounds at the first debridement. Additionally, at the first debridement, gene expression of type IV collagen  $\alpha 3$  (COL4A3) is twofold up-regulated in impaired healing wounds compared with normal healing wounds. A similar gene expression profile with reduced expression of COL1A1 and COL3A1 is observed for the second debridement biopsies (Figure 3B). As shown in Figure 3C, by the third debridement, gene expression for COL18A1 (type XVIII collagen  $\alpha 1$ ) is up-regulated by twofold for impaired healing wounds compared with normal healing wounds, as well as for COL4A1 (type IV collagen  $\alpha 1$ ). By the final debridement (Figure 3D), only COL18A1 shows an up-regulation in impaired healing wounds compared with normal healing wounds, while COL1A1, COL3A1, COL4A1, COL4A3 are expressed at similar levels in normal and impaired healing wounds. In general, COL18A1 is up-regulated at almost all time points for impaired healing wounds compared with normal healing wounds.

#### Raman mapping of wound tissue biopsy sections

For this proof-of-principle study, a smaller cohort of patients was chosen for Raman spectroscopic mapping of wound biopsies ( $n=10$ ). Wound biopsies were mapped

with Raman spectroscopy for nine patients at two time points—first debridement and last debridement. Of the 10 biopsy series, four sets of biopsies were classified as normal healing and three sets of biopsies were classified as impaired healing. A visible image collected for a tissue section of a normal healing wound biopsy at the first debridement is shown in Figure 4A. The yellow crosses indicate each position where a Raman spectrum was acquired. The corresponding score image and loading are shown in Figure 4B and C. Red pixels indicate high intensity and blue pixels indicate lowest intensity—note, the pixels with highest intensities correlate with the wound biopsy, while the background (the aluminized slide) has the lowest intensity. The loading most closely resembles a Raman spectrum of tissue, largely proteinaceous in origin. A similar visible image, score image, and loading were also obtained for the final debridement wound biopsy (Figure 4D–F, respectively).

Prominent Raman bands in the loading can be assigned to peaks often found in tissue (see Table 2):  $-860\text{ cm}^{-1}$  (hydroxyproline),  $920\text{ cm}^{-1}$  (proline),  $1,004\text{ cm}^{-1}$  (phenylalanine),  $1,030$  and  $1,070\text{ cm}^{-1}$  (nucleic acids),  $1,240$  and  $1,270\text{ cm}^{-1}$  (proteins, Amide III),  $\sim 1,300\text{ cm}^{-1}$  (proteins, nucleic acids),  $1,445\text{ cm}^{-1}$  (proteins),  $1,609\text{ cm}^{-1}$  (aromatic amino acids), and  $1,665\text{ cm}^{-1}$  (proteins, Amide I). A loading for the tissue component and a corresponding score image were obtained for each wound biopsy,

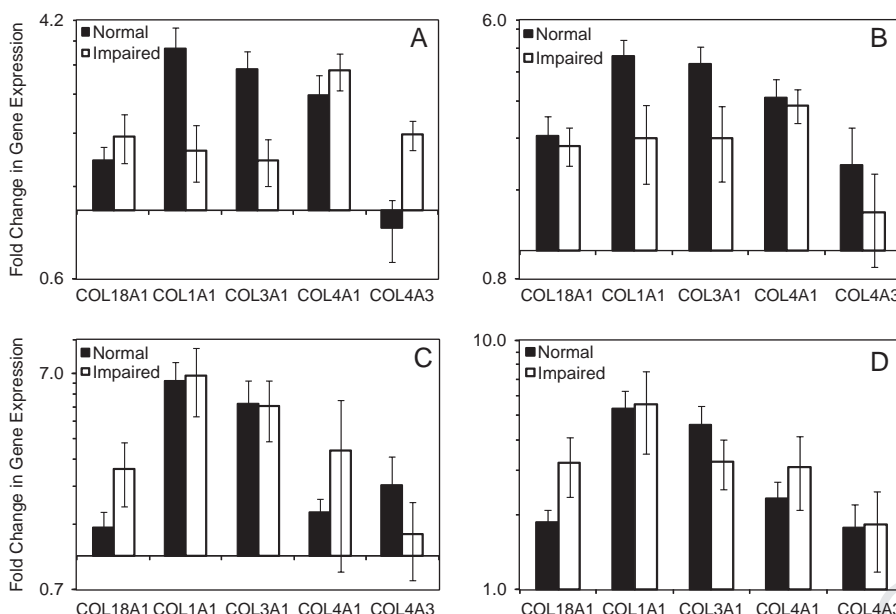


**Figure 3.** Comparison of fold change difference in collagen gene expression for normal and impaired wound healing at the first (A), second (B), third (C), and last (D) debridements. Error bars indicate the standard error of mean.

similar to those shown in Figure 4. Curve fitting was performed for each tissue component loading, to elucidate any changes in tissue composition of the wound biopsies between the first and last debridements. More specifically, the ratio of the Amide I band area ( $\sim 1,665\text{ cm}^{-1}$ ) to the  $\text{CH}_2$  scissoring band area ( $\sim 1,445\text{ cm}^{-1}$ ) was calculated. The band area of the methylene scissoring vibrational band is reflective of the total protein content, while the band area of the Amide I vibrational band, specifically located at  $\sim 1,665\text{ cm}^{-1}$ , is reflective of the collagen content. Thus, an increase in collagen content would be indicated by a larger  $1,665/1,445\text{ cm}^{-1}$  band area ratio. Percent differences in these ratios for the first and last debridements are shown in Figure 5. For six of the wound biopsy sets, the  $1,665/1,445\text{ cm}^{-1}$  band area ratio is significantly

decreased for the last debridement, with percent differences of  $-63.1$ ,  $-34.6$ ,  $-26.7$ ,  $-41.1$ ,  $-42.9$ , and  $-52.6\%$ . Four of the wound biopsy sets have positive or minimally negative changes in the band area ratios with percent differences of  $-1.8$ ,  $2.7$ ,  $15.4$ , and  $34.0\%$ .

## DISCUSSION

Currently, wounds are evaluated using parameters such as location of injury, adequacy of perfusion, gross appearance of the wound, wound tensile strength, and the patient's general condition. While parameters such as the location of injury, gross appearance of the wound, and the patient's general condition are fairly obvious and reasonably assessed, parameters such as adequacy of perfusion

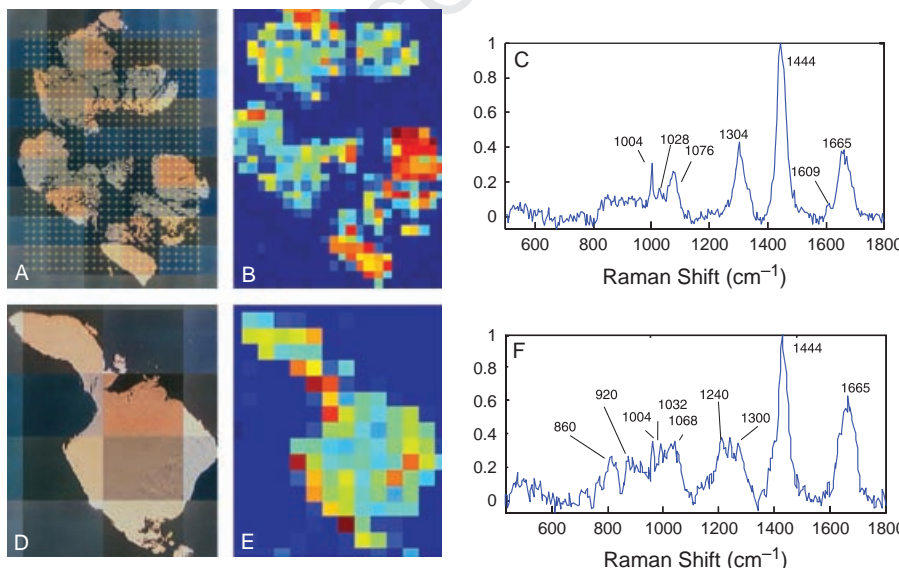


**Figure 4.** Visible images of tissue sections for a normal healing wound at first (A) and last (D) debridements. Corresponding score images (B and E) and components are displayed (C and F) for each tissue biopsy section, taken at the first and last debridements, respectively. Each pixel in the score image is approximately  $100 \times 100\text{ }\mu\text{m}$ .

**Table 2.** Raman vibrational band assignments<sup>31–32</sup>

Raman shift (cm <sup>-1</sup> )	Vibrational band assignment	Component
860	v (C–C)	Nucleic acids
920	v (C–N), v (C–C)	Nucleic acids, keratin
1,004	v (C–C) ring	Phenylalanine
1,030	v (C–C) skeletal	Nucleic acids, protein
1,070	v (C–C) skeletal	Nucleic acids, protein
1,240, 1,270	v (C–N) and δ(N–H); Amide III	Protein
1,300	δ (CH <sub>2</sub> ) twisting	Nucleic acids, protein
1,445	δ (CH <sub>3</sub> ) and δ (CH <sub>2</sub> ) scissoring	Protein
1,609		Aromatic amino acids
1,665	v (C=O); Amide I	Protein

and tensile strength are not readily quantifiable during surgery. It has been previously demonstrated that there is a greater incidence of associated vascular injury in delayed healing wounds when compared with normal healing wounds. It is also well established that tensile strength of the wound is dependent on collagen deposition.<sup>29</sup> There exists a need for technologies that can noninvasively and objectively assess these challenging parameters.

In this preliminary study, Raman spectroscopic mapping of tissue biopsies collected during the wound healing process reveals a decrease in the 1,665/1,445 cm<sup>-1</sup> band

area ratios of impaired healing wounds compared with normal healing wounds. Using the 1,445 cm<sup>-1</sup> band area as an indicator of overall proteinaceous content and the 1,665 cm<sup>-1</sup> band area as a measure of collagen content, one can monitor collagen deposition in the wound biopsies, utilizing the 1,665/1,445 cm<sup>-1</sup> band area ratio. Thus, the decrease in the 1,665/1,445 cm<sup>-1</sup> band area ratios is an indication of impaired collagen deposition in wounds that are classified as impaired healing wounds.

Gene profiles of mRNA extracted from the wound biopsies corroborate the results of the Raman spectroscopic maps. COL1A1 and COL3A1 mRNA expression profiles were initially decreased in impaired healing wounds when compared with normal healing wounds. In early wound healing, type III collagen is most abundant and is gradually replaced by type I collagen. COL3A1 encodes for the pro- $\alpha$ 1(III) chains, which are the building block of type III collagen. COL1A1 encodes for the pro- $\alpha$ 1(I) chains, which are used to form type I collagen fibrils. Type I collagen is the most abundant form of collagen in the body, serving as the framework for connective tissues such as skin, bone, cartilage, and tendons. An initial reduction in the expression of COL3A1 could hinder deposition of type III collagen in the wound bed, which, in turn, would delay deposition of type I collagen, a key step in reepithelialization. As observed in the larger cohort of patients, impaired healing wounds show a twofold decrease in up-regulation of COL1A1 and COL3A1 genes in the beginning of the wound healing process, compared with normal healing wounds. COL18A1 encodes for an ECM protein, endostatin, which is an inhibitor of angiogenesis. COL18A1 mRNA expression remains elevated for impaired healing wounds at almost all time points when compared with normal healing wounds. Continued elevation of endostatin would inhibit neovascularization, which is observed in the pathology of the tissue sections in this study. COL4A1 and COL4A3 encode the pro- $\alpha$ 1(IV) chains and pro- $\alpha$ 3(IV) chains, respectively, found in basement membranes such as the epidermal basement membrane. Elevated COL4A1 and COL4A3 levels may, however, also act as inhibitors of angiogenesis.

In chronic wounds, proinflammatory cytokines have been identified as potent stimulators of matrix metalloproteinases (MMPs). MMP-13 (collagenase 3), however, is significantly decreased in impaired healing wounds and wound effluent. Collagenase 3 digests type III collagen in the wound bed. This is a critical step in the wound healing process; fibroblasts enter the maturation stage of healing and lay down type I collagen in the wound only after much of the type III collagen has been removed.<sup>4</sup> Thus, a reduced MMP-13 mRNA expression could directly impact wound tensile strength. In a study by Hartenstein et al.,<sup>30</sup> mice deficient in MMP-13 exhibited elevated levels of MMP-8. In this study, patients with impaired healing wounds also exhibited elevated levels of MMP-8.

An amplified inflammatory response can result in disrupted or altered cytokine and chemokine signaling, preventing a normal progression into the fibroproliferative phase of wound healing. Previous models of acute wound healing have demonstrated abnormal collagen metabolism, a result of either decreased collagen synthesis or increased protease activity. This ultimately creates an imbalance during matrix formation and homeostasis,

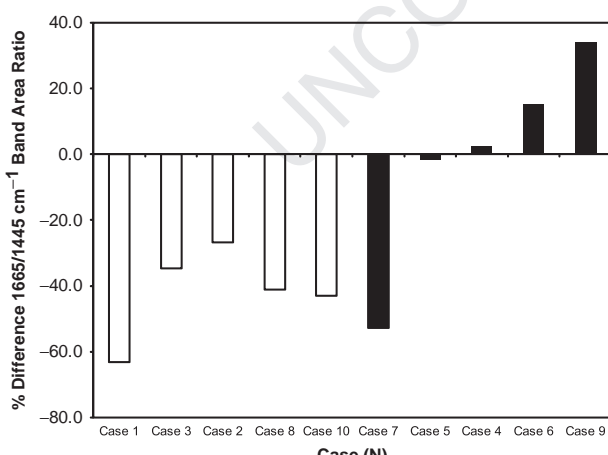


**Figure 5.** The percent difference of the 1,665/1,445 cm<sup>-1</sup> band area ratios calculated from the first and last debridements 1,665/1,445 cm<sup>-1</sup> band area ratios for wounds classified as normal healing (black bars) and as impaired healing (white bars).

causing decreased collagen levels, reduced wound mechanical strength, and finally wound failure.<sup>6</sup> In this study, patients with impaired healing wounds demonstrate exactly that, evidenced by the decrease in the 1,665/1,445 cm<sup>-1</sup> band area ratios, revealing decreased collagen content in tissue biopsies taken directly from the wound bed. Based on the Raman spectroscopic results only, however, one of the normal healing wounds would have been classified as an impaired healing wound. For this small cohort of patients, wounds classified clinically as normal healing wounds were defined as wounds from patients who had a mean hospital stay of < 21 days, while wounds classified clinically as impaired healing wounds were defined as wounds from patients who had a mean hospital stay of > 21 days. The seventh case, classified clinically as normal healing, exhibited a significant loss in collagen content of the wound bed from the first surgical debridement to the last surgical debridement, specifically -52.6%. This patient was hospitalized for 18 days, just 3 days less than the clinical classification for impaired wound healing.

In this study, Raman spectroscopic maps of sectioned wound tissue from nine patients were collected and analyzed, to compare the chemical compositions of normal healing wound tissue and of impaired healing wound tissue. Although all data acquisition and analysis were performed outside of the surgical arena, it is possible to incorporate similar Raman spectroscopic equipment into the operating room. First, Raman spectroscopy can be used in a noninvasive manner, such as a fiber probe-coupled system. Second, based on the fiber probe design itself, the Raman spectroscopic system could sample a tissue volume of up to ~60 mm<sup>3</sup>, or greater; a standard punch biopsy samples approximately 140 mm<sup>3</sup> of tissue. Once a significant database of samples and their corresponding Raman factors have been collected, it is possible to develop an algorithm capable of monitoring collagen levels in the wounds bed. Although the cohort of patients examined here was small and preliminary, the results are encouraging. This study shows the potential of Raman spectroscopy as a technique capable of affording an objective measurement regarding wound healing in the operating room. Such a capability would allow for real-time point of care analysis of wounds, allowing subjective decisions to be supplanted by objective data. This is a critical need as constraints on surgical education reduce operative exposure and clinical decision-making is moved from the subjective arena to data-driven decisions. The use of such methodologies as presented herein, may allow for fewer trips to the operating room, reduced costs, and faster rehabilitation in both military and civilian traumatic wounds. In order to reach this potential, future work will need to expand the number of patients in the study to better delineate Raman spectroscopic trends during the wound healing process. Additional cases could help define a threshold to classify wounds as normal healing or impaired healing, based on Raman spectral results.

## ACKNOWLEDGMENTS

The authors would like to thank Dr. Thomas Davis for his role in developing the gene expression assay used in this manuscript. This work was prepared as part of the au-

thors' official duties. Title 17 U.S.C. §105 provides that "Copyright protection under this title is not available for any work of the United States Government." Title 17 U.S.C. §101 defines a US Government work as a work prepared by a military service member or employee of the US Government as part of that person's official duties. The views expressed in this article are those of the author and do not necessarily reflect the official policy or position of the Department of the Navy, Department of Defense, nor the US Government. This work was supported and funded by work unit number 604771N.0933.001.A0604.

## REFERENCES

1. Owens BD, Kragh JF Jr., Wenke JC, Macaitis J, Wade CE, Holcomb JB. Combat wounds in operation Iraqi freedom and operation enduring freedom. *J Trauma* 2008; 64: 295–9.
2. Eming SA, Krieg T, Davidson JM. Inflammation in wound repair: molecular and cellular mechanisms. *J Invest Dermatol* 2007; 127: 514–25.
3. Haworth JS, Stojadinovic A, Gage FA, Tadaki DK, Perdue PW, Forsberg J, Davis TA, Dunne JR, Denobile JW, Brown TS, Elster EA. Inflammatory biomarkers in combat wound healing. *Ann Surg* 2009; 250: 1002–7.
4. Witte MB, Barbul A. General principles of wound healing. *Surg Clin North Am* 1997; 77: 509–28.
5. Broughton G II, Janis JE, Attinger CE. The basic science of wound healing. *Plast Reconstr Surg* 2006; 117 (Suppl.): 12S–34S.
6. Dubay DA, Franz MG. Acute wound healing: the biology of acute wound failure. *Surg Clin North Am* 2003; 83: 463–81.
7. Wills H, Kast R, Stewart C, Rabah R, Pandya A, Poulik J, Auner G, Klein MD. Raman spectroscopy detects and distinguishes neuroblastoma and related tissues in fresh and (banked) frozen specimens. *J Pediatr Surg* 2009; 44: 386–91.
8. Harvey TJ, Faria EC, Henderson A, Gazi E, Ward AD, Clarke NW, Brown MD, Snook RD, Gardner P. Spectral discrimination of live prostate and bladder cancer cell lines using Raman optical tweezers. *J Biomed Opt* 2008; 13: 064004.
9. Andrade PO, Bitar RA, Yassoyama K, Martinho H, Santo AM, Bruno PM, Martin AA. Study of normal colorectal tissue by FT-Raman spectroscopy. *Anal Bioanal Chem* 2007; 387: 1643–8.
10. Buschman HP, Deinum G, Motz JT, Fitzmaurice M, Kramer JR, van der Laarse A, Bruschke AV, Feld MS. Raman microspectroscopy of human coronary atherosclerosis: biochemical assessment of cellular and extracellular morphologic structures in situ. *Cardiovasc Pathol* 2001; 10: 69–82.
11. Carden A, Rajachar RM, Morris MD, Kohn DH. Ultrastructural changes accompanying the mechanical deformation of bone tissue: a Raman imaging study. *Calcif Tissue Int* 2003; 72: 166–75.
12. Chan KL, Zhang G, Tomic-Canic M, Stojadinovic O, Lee B, Flach CR, Mendelsohn R. A coordinated approach to cutaneous wound healing: vibrational microscopy and molecular biology. *J Cell Mol Med* 2008. Epub August 9, 2008.
13. Chowdary MV, Kumar KK, Thakur K, Anand A, Kurien J, Krishna CM, Mathew S. Discrimination of normal and malignant mucosal tissues of the colon by Raman spectroscopy. *Photomed Laser Surg* 2007; 25: 269–74.
14. Crane NJ, Popescu V, Morris MD, Steenhuis P, Ignelzi MA Jr. Raman spectroscopic evidence for octacalcium phosphate

Q1

Q2

and other transient mineral species deposited during intramembranous mineralization. *Bone* 2006; 39: 434–42.

15. Haka AS, Volynskaya Z, Gardecki JA, Nazemi J, Lyons J, Hicks D, Fitzmaurice M, Dasari RR, Crowe JP, Feld MS. In vivo margin assessment during partial mastectomy breast surgery using Raman spectroscopy. *Cancer Res* 2006; 66: 3317–22.
16. Jess PR, Smith DD, Mazilu M, Dholakia K, Riches AC, Herrington CS. Early detection of cervical neoplasia by Raman spectroscopy. *Int J Cancer* 2007; 121: 2723–8.
17. Koljenović S, Schut TC, Wolthuis R, Vincent AJ, Hendriks-Hagevi G, Santos L, Kros JM, Puppels GJ. Raman spectroscopic characterization of porcine brain tissue using a single fiber-optic probe. *Anal Chem* 2007; 79: 557–64.
18. Leroy G, Penel G, Leroy N, Brès E. Human tooth enamel: a Raman polarized approach. *Appl Spectrosc* 2002; 56: 1030–4.
19. McGill N, Dieppe PA, Bowden M, Gardiner DJ, Hall M. Identification of pathological mineral deposits by Raman microscopy. *Lancet* 1991; 337: 77–8.
20. Robichaux-Viehoever A, Kanter E, Shappell H, Billheimer D, Jones H III, Mahadevan-Jansen A. Characterization of Raman spectra measured in vivo for the detection of cervical dysplasia. *Appl Spectrosc* 2007; 61: 986–93.
21. Shetty G, Kendall C, Shepherd N, Stone N, Barr H. Raman spectroscopy: elucidation of biochemical changes in carcinogenesis of oesophagus. *Br J Cancer* 2006; 94: 1460–4.
22. Shim MG, Wilson BC, Marple E, Wach M. Study of fiber-optic probes for in vivo medical Raman spectroscopy. *Appl Spectrosc* 1999; 53: 619–27.
23. Wang TD, Van Dam J. Optical biopsy: a new frontier in endoscopic detection and diagnosis. *Clin Gastroenterol Hepatol* 2004; 2: 744–53.
24. Chen G, Chen J, Zhuo S, Xiong S, Zeng H, Jiang X, Chen R, Xie S. Nonlinear spectral imaging of human hypertrophic scar based on two-photon excited fluorescence and second-harmonic generation. *Br J Dermatol* 2009; 161: 48–55.
25. Livak KJ, Schmittgen TD. Analysis of relative gene expression data using real-time quantitative PCR and the 2(-Delta Delta C(T)) Method. *Methods* 2001; 25: 402–8.
26. Ong LR, Widjaja E, Stanforth R, Garland M. Fourier transform Raman spectral reconstruction of inorganic lead mixtures using a novel band-target entropy minimization (BTEM) method. *J Raman Spectrosc* 2003; 34: 282–9.
27. Widjaja E, Crane N, Chen T, Morris MD, Ignelzi MA Jr., McCreadie B. Band-target entropy minimization (BTEM) applied to hyperspectral Raman image data. *Appl Spectrosc* 2003; 57: 1353–62.
28. Widjaja E, Li C, Chew W, Garland M. Band-target entropy minimization. A robust algorithm for pure component spectra recovery. Application to complex randomized mixtures of six components. *Anal Chem* 2003; 75: 4499–507.
29. Brunicardi FC, Andersen D, Billiar T, Dunn D, Hunter J, Pollock R. *Schwartz's manual of surgery*. New York, NY: The McGraw-Hill Companies, 2006: 2000.
30. Hartenstein B, Dittrich BT, Stickens D, Heyer B, Vu TH, Teurich S, Schorpp-Kistner M, Werb Z, Angel P. Epidermal development and wound healing in matrix metalloproteinase 13-deficient mice. *J Invest Dermatol* 2006; 126: 486–96.
31. Tarakeshwar P, Manogaran S. Proline and hydroxyproline zwitterions—an ab initio study. *J Mol Struct (Theochem)* 1997; 417: 255–63.
32. Frushour BG, Koenig JL. Raman scattering of collagen, gelatin, and elastin. *Biopolymers* 1975; 14: 379–91.

Q3